Supporting Information

TITLE: In Situ Ligand-Directed Growth of Gold Nanoparticles in Biological Tissues

AUTHORS: *Chuanqi Peng, Mengxiao Yu, Jie Zheng**

AFFILIATION(S): Department of Chemistry and Biochemistry, The University of Texas at Dallas, 800 W. Campbell Road, Richardson, TX 75080, United States

*Correspondence to: jiezheng@utdallas.edu

KEYWORDS: Gold nanoparticles, growth, in situ, imaging, staining, tissue engineering

Table of Contents

Methods

Materials. Gold(III) chloride trihydrate ($HAuCl_4$), L-glutathione reduced (GSH), poly(ethylene glycol) methyl ether thiol (mPEG-SH, m.w. 800 Da), β-glucose thiol (1-thio-β-D-glucose sodium salt), neutralized 4% formaldehyde (also known as 10% formalin), Tris(2-carboxyethyl)phosphine hydrochloride (TCEP·HCl), 4',6-diamidino-2-phenylindole (DAPI) and other chemicals were purchased from Sigma-Aldrich (St. Louis, MO, USA) unless otherwise stated. Osmium tetroxide (OsO_4, 4% aqueous solution) for electron microscopy staining was purchased from Electron Microscopy Sciences.

Controlled growth of thiolated gold nanoparticles (AuNPs) in solution. The AuNP growth in the presence of different thiol ligands (GSH and mPEG-SH) was initially investigated by using various gold-to-thiol ratios as well as different pH values (see **Fig. S1** and **S4**). Under predetermined conditions (for instance, gold-to-thiol ratio of 1:1 in neutral pH for GSH ligand, 0.5 mM), the nanoparticle formation processes with different ligands in solution can be optimized under controlled kinetics for further in situ growth in biological tissues and characterization with transmission electron microscopy (TEM). In addition, the ultrasmall AuNPs (<5 nm) with near-infrared (NIR) luminescence can be formed in the early formation phase using predefined stoichiometry and pH for different thiols, where the photoluminescence was monitored with a spectrophotometer. The 4% formaldehyde was used as the reducing agent[1] for the controllable reduction of GSH-coated AuNPs (GS-AuNPs) and mPEG-SH-coated AuNPs (mPEG-AuNPs), and TCEP·HCl was used for decelerating the reduction process[2] of β-glucose thiol-coated AuNPs (β-glucose-AuNPs).

In situ growth of thiolated AuNPs in biological environment (tissues). For the in situ growth of GS-AuNPs or mPEG-AuNPs in biological tissues such as kidney and brain, pre-fixed tissue sections (from 4 μm up to 1 mm, for either newly fixed tissues or formalin-fixed paraffin-embedded, FFPE, tissues) were immersed in neutralized 4% formaldehyde in petri-dish and the selected thiol (R-SH, initially GSH) was added into the solution to a final concentration of 0.5 mM. The solution was then mixed gently by swirling

and incubated for 30 min at room temperature. Next, $HAuCl_4$ in pure water was then added into the solution to the predetermined gold-to-thiol ratio (**Fig. S1** and **S4**) and the solution was gently mixed again by swirling. The solution showed the transparent to light yellow color after the addition of $HAuCl_4$, which then turned into light brown-red after 1-day incubation at room temperature, indicating the formation of AuNPs with ultrasmall sizes (<5 nm). With time proceeded, the solution would change the color into red, indicating the evolution of AuNPs from ultrasmall to larger size (>5 nm, plasmonic AuNPs). On day 2, specific regions of tissues (kidney, initially) could be stained with red color for direct observation and further characterization, which found no changes after 2 days due to the depletion of thiolated gold precursor ([Au-SR]) in solution. For the in situ formation of AuNPs with β-glucose thiol (β-glucose-SH), the fixed tissues were immersed in pure water (instead of 4% formaldehyde) and β-glucose thiol was added to a final concentration of 0.25 mM. After incubation for 30 min at room temperature, $HAuCl_4$ and TCEP (1:2, TCEP was used to decelerate the reduction[2]) in pure water were premixed and added into the solution to a final gold-to-thiol molar ratio of 1:0.25 (1 mM for $HAuCl_4$) and the solution was gently mixed by swirling. For in situ growth of β-glucose-AuNPs, the tissues were incubated and characterized followed the same procedure.

Characterization and size analysis of in situ formed AuNPs with electron microscopy imaging. After the successful growth of plasmonic AuNPs in the biological tissues, the animal tissues (1 mm thickness) with grown AuNPs were washed with pure water to remove any free nanoparticles, stained with osmium tetroxide (OsO_4), dehydrated and embedded in epoxy resin, sectioned into slides of 50-nm thickness and imaged with biological TEM (JEOL 1400 transmission electron microscope). Blank tissues without AuNP growth were processed the same as control group. After 2-day nanoparticle growth, the plasmonic AuNPs in kidney and brain tissues are of sizes above 10 nm, which can be readily viewed and analyzed on the tissues from TEM imaging. Nano Measurer software was used for the size distribution analysis.

Characterization of in situ formed AuNPs with near-infrared (NIR) imaging. With precise control of the NP formation kinetics, the ultrasmall AuNPs with NIR luminescence can be formed in the tissues in the early formation process (day 1). After the in situ formation of NIR luminescent AuNPs, the animal tissues were then washed with pure water to remove non-specific contents and mounted with DAPI-containing aqueous gel on glass slides for fluorescence microscopy imaging (Olympus IX71 inverted microscope) and confocal fluorescence microscopy imaging (Olympus FV3000RS laser scanning confocal microscope). The luminescence spectra were collected by a PTI QuantaMaster^{TM} 30 Fluorescence Spectrophotometer.

Statistics. For the statistical analysis, Student's t-test was used to assess the statistical significance between two groups. One-way ANOVA was used to compare among multiple groups.

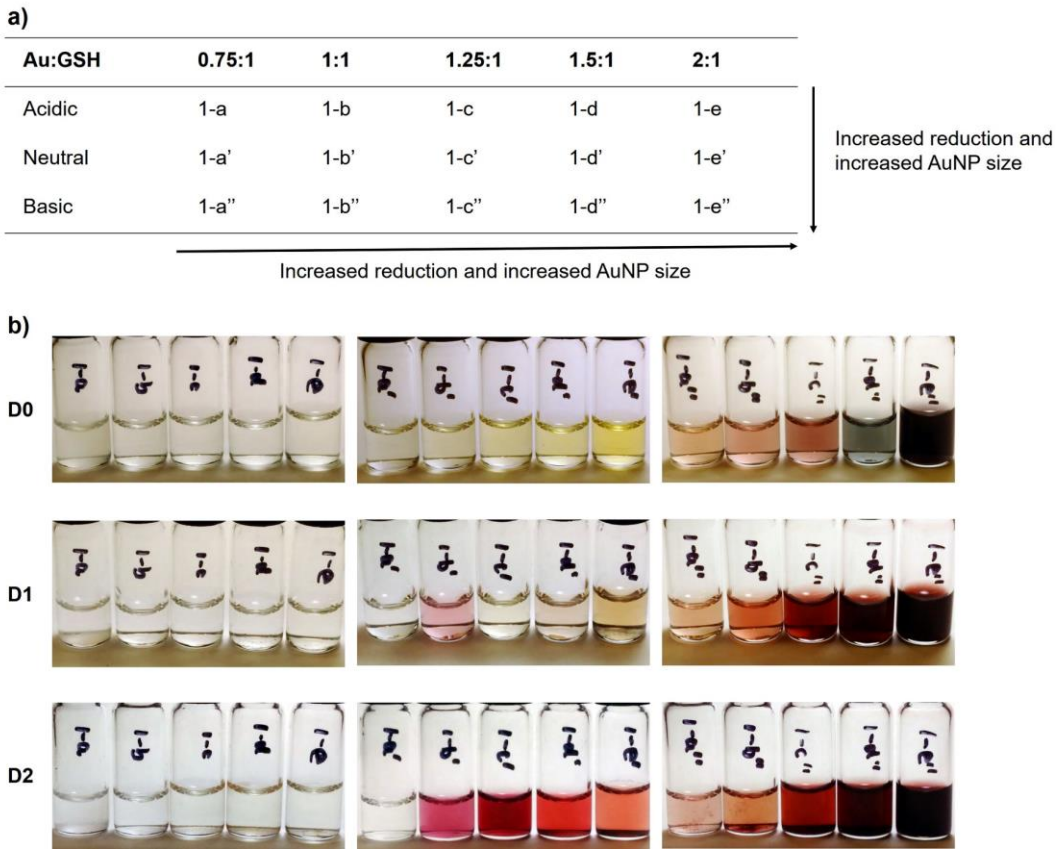

Figure S1. Growth of GS-AuNPs in solution under different conditions. The GS-AuNPs were synthesized under different gold-to-thiol (Au:GSH) ratio and pH conditions (**a**), where the increased Au:GSH ratio and pH value were found to increase both the reduction rates and AuNP sizes (**b**). In addition, the reduction of the formaldehyde[1] concentration could decrease the reduction rate. For the in situ GSH-directed AuNP growth on biological tissues, Au:GSH ratio of 1:1 and a neutral pH (**trial 1-b'**) was chosen.

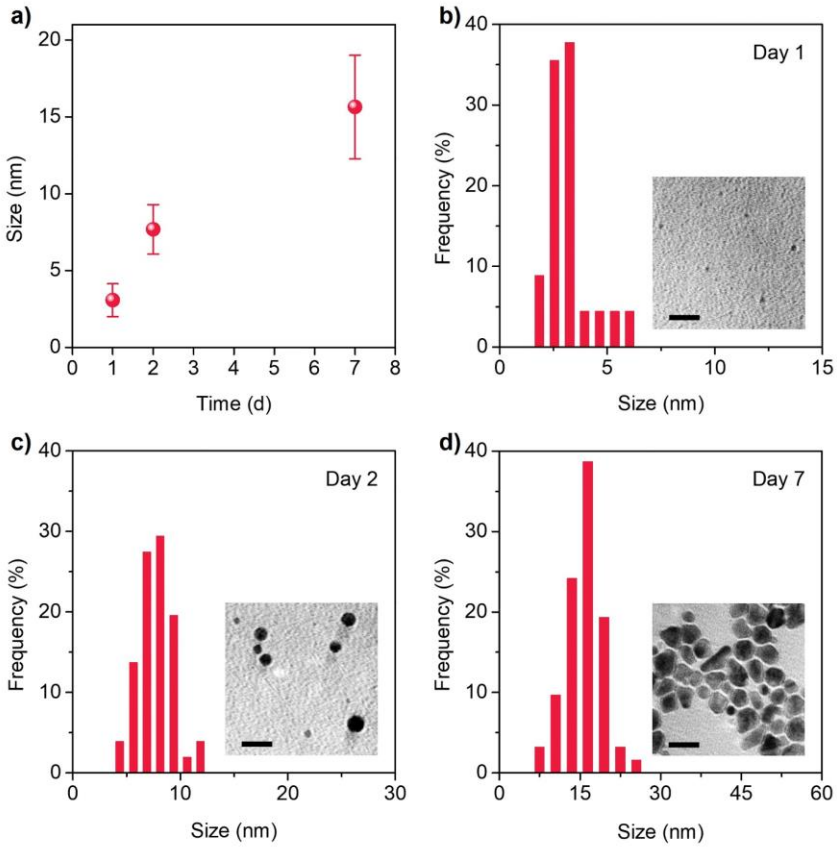

Figure S2. Size evolution of GS-AuNPs at different time points. Based on the predetermined condition (trial 1-b' in **Fig. S1**), the GS-AuNPs gradually formed and evolved with larger size within a week (**a**), which were then characterized with TEM imaging at select time points (Day 1, Day 2 and Day 7). The GS-AuNPs were of ultrasmall size (3.08 ± 1.07 nm, **b**) on Day 1, which then evolved into a larger size (7.68 ± 1.60 nm, **c**) on Day 2. After 7 days, the GS-AuNPs could grow as large as (15.64 ± 3.37 nm, **d**). Scale bar, 20 nm.

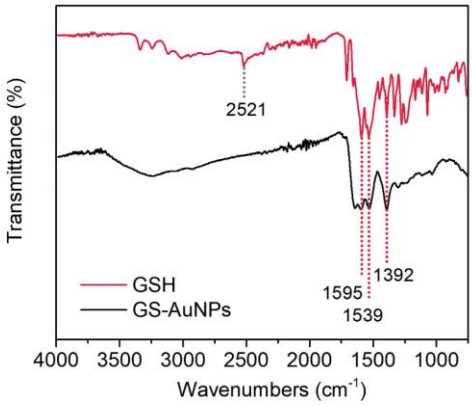

Figure S3. FT-IR spectra of the GS-AuNPs and GSH. The AuNPs (purified and lyophilized) were prepared 2 d after the incubation of $HAuCl_4$ with GSH in solution in the presence of 4% formaldehyde. For the formed GS-AuNPs, the absorption bands of the -COO- group (~1595 cm^{-1}) and amide group (~1539 cm^{-1}) indicated the GSH coating on the AuNPs.[3] Moreover, compared to free GSH, the characteristic absorption peak of S-H stretching band (2521 cm^{-1}) disappeared due to the formation of Au-S bonding on NPs. The results indicated that the GSH molecules in the solution were used to coat and stabilize the formed AuNPs.

a)

Au:mPEG-SH	0.75:1	1:1	1.25:1	1.5:1	2:1
Acidic	2-a	2-b	2-c	2-d	2-e
Neutral	2-a'	2-b'	2-c'	2-d'	2-e'
Basic	2-a''	2-b''	2-c''	2-d''	2-e''

Increased reduction and increased AuNP size

Increased reduction and increased AuNP size

b)

Figure S4. Growth of mPEG-AuNPs in solution under different conditions. Similar to GS-AuNPs, the mPEG-AuNPs could be synthesized under different gold-to-thiol ratio (Au:mPEG-SH) and pH conditions (**a**), where the increased Au:mPEG-SH ratio and pH value were found to increase both the reduction rates and AuNP sizes (**b**). To be noted, the Au-SR reduction and AuNP formation were found to be slightly slower for mPEG-SH than GSH. The condition under Au:mPEG ratio of 1:1 and a neutral pH (**trial 2-b'**) was found to exhibit strong near-infrared (NIR) luminescence as well, which was used for the in situ growth of mPEG-AuNPs on tissues.

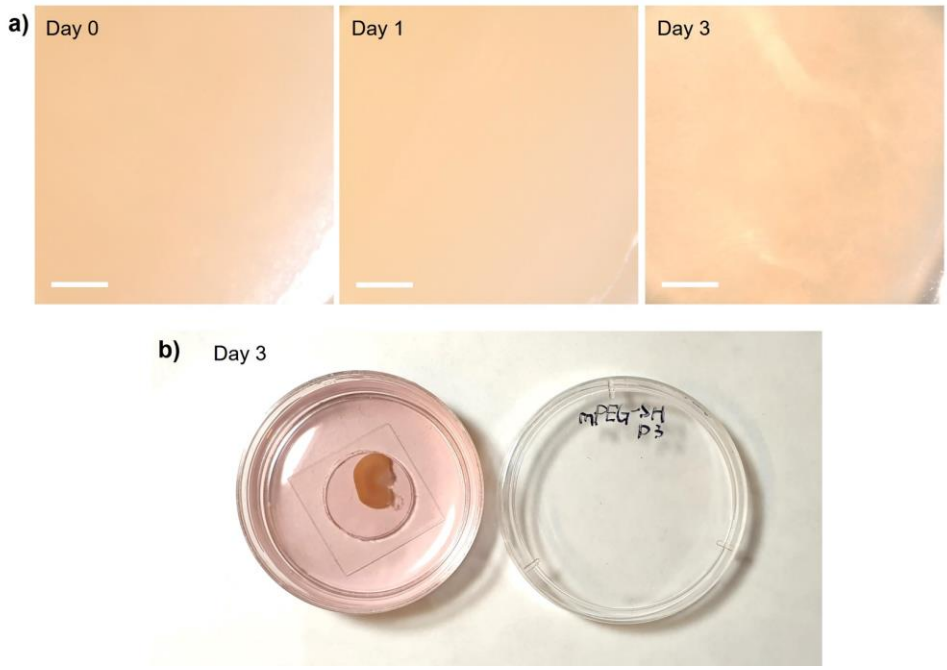

Figure S5. Evolution process of the in situ growth of mPEG-AuNPs in the kidney tissues. a) In contrast to GS-AuNPs, the mPEG-AuNPs were found to have low affinity to and minimal distribution in kidney tissue, where no plasmonic mPEG-AuNPs was found to form in the tissue under the same condition. Scale bar, 0.2 mm. **b**) With time proceeded after 3 days, there were plasmonic mPEG-AuNPs readily visualized in solution, however, there still were no observable plasmonic mPEG-AuNPs in the tissues, indicating the low affinity and specificity of the mPEG-SH ligand towards the same tissue. Moreover, minimal change was found in the colors of solution and tissues after Day 3.

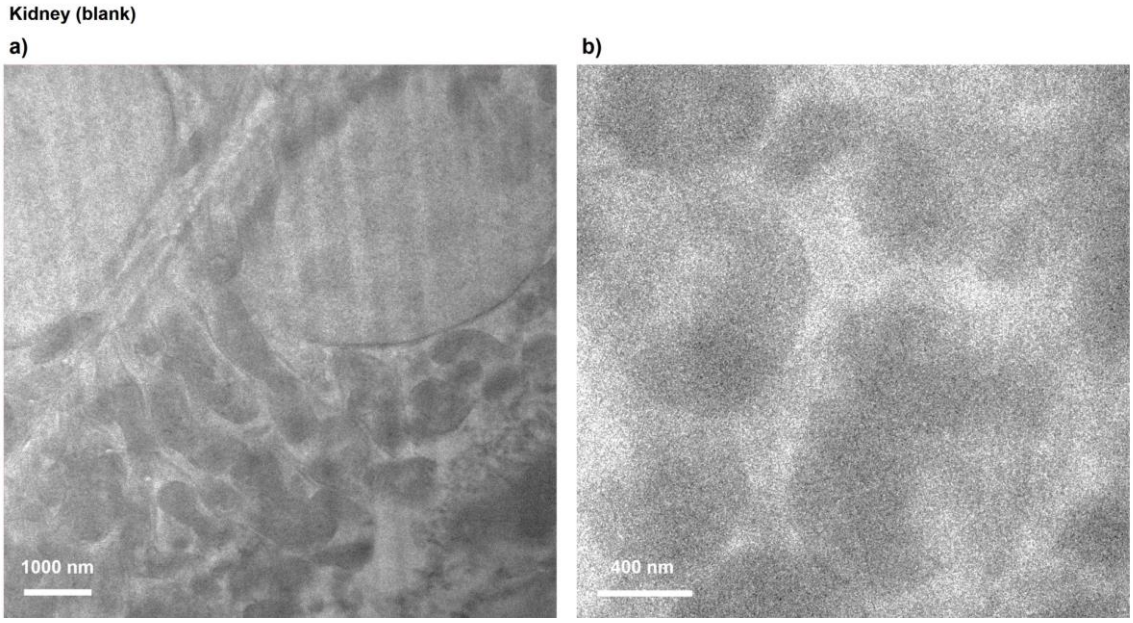

Figure S6. TEM imaging of the kidney (blank) without the growth of GS-AuNPs. There are no nanoparticle-like signals from the blank kidney tissues and the mitochondria in blank tissues (**b**) were of lower contrast due to no nanoparticle staining.

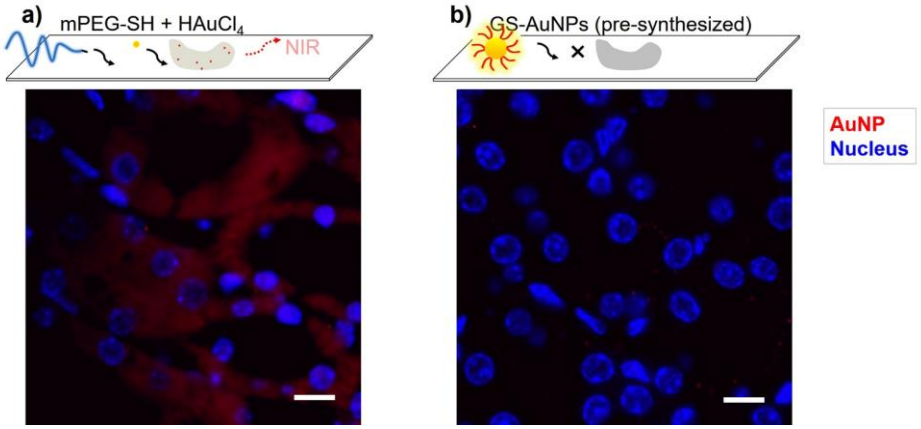

Figure S7. NIR fluorescence microscopy imaging of the different kidney tissues. a) In the early formation phase, compared to the in situ growth of ultrasmall NIR luminescent GS-AuNPs (**Fig. 3d**), the AuNP growth in the presence of non-specific mPEG-SH ligand showed low in situ formation, and more importantly, no preferential distribution of mPEG-AuNPs in the same tissues (notably, mPEG-AuNPs with comparable NIR luminescence can also be synthesized under the same condition with GS-AuNPs). In addition, some control thiols, such cysteine, thioguanosine, mercaptobenzoic acid, etc., could not induce the selective AuNP growth in tissues as well. **b**) The pre-synthesized NIR luminescent GS-AuNPs (of the same amount) also showed quite low distribution in kidney tissues, indicating there was no strong interaction between the kidney and the GS-AuNPs formed in solution. Scale bar, 10 μm.

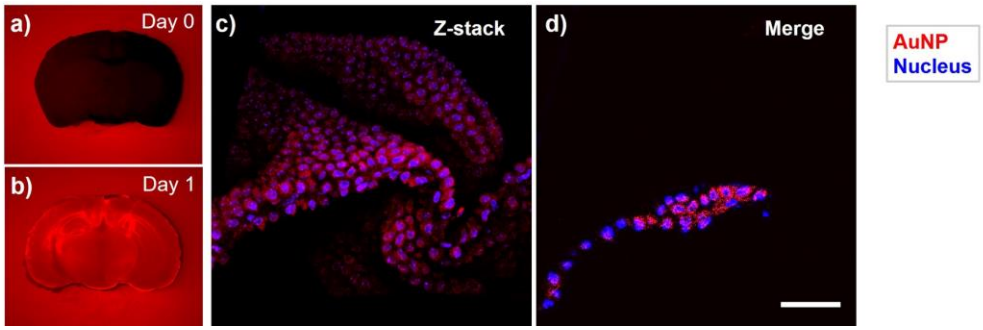

Figure S8. NIR fluorescence microscopy imaging of the in situ formed GS-AuNPs in brain hippocampus. a-b) Whole-tissue NIR imaging of the brain before (Day 0, **a**) and after (Day 1, **b**) NP growth. There were strong NIR signals in the brain slides, especially in the hippocampus area, 1 day after the GSH-directed AuNP growth, indicating the selective distribution of GS-AuNPs in brain hippocampus in addition to the renal tubules. **c-d**) Confocal fluorescent microscopy imaging (Z-stack, **c** and 2D merge, **d**) of GS-AuNPs in hippocampus cells (in the DG area). Full-scale width, 320 µm for **c**; Scale bar, 50 µm for **d**.

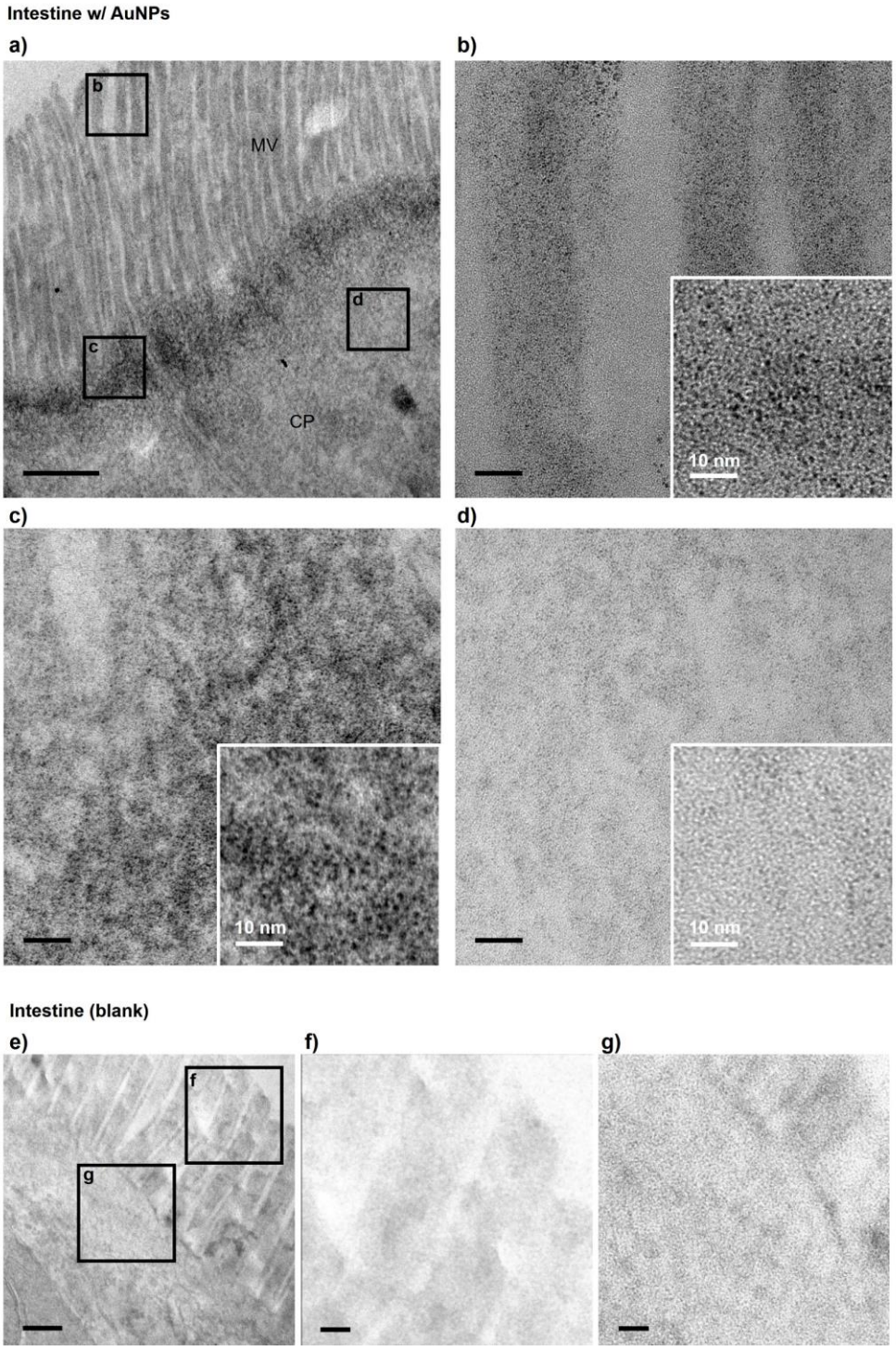

Figure S9. TEM imaging of the small intestine with and without in situ growth of β-glucose-AuNPs. **a-d**) TEM imaging of the mucosa cells in small intestine with in situ growth of AuNPs, showing the significant distribution of β-Glucose-AuNPs on the microvilli (MV in **a**, and **b**) and cellular membrane (next to the MV, **c**) of these mucosa cells, whereas, the cytoplasm of small intestine (CP in **a**, and **c**) showed low AuNP distribution. To be noted, the β-glucose-AuNPs showed faster kinetics of NP formation

and smaller NP sizes than GS-AuNPs**.** Scale bars, 500 nm for **a**, 50 nm for **b**-**d**. In contrast, the intestine (blank) was shown as **e**-**g**, which showed a lower contrast with no NPs. Scale bars, 200 nm for **e**, 50 nm for **f** and **g**.

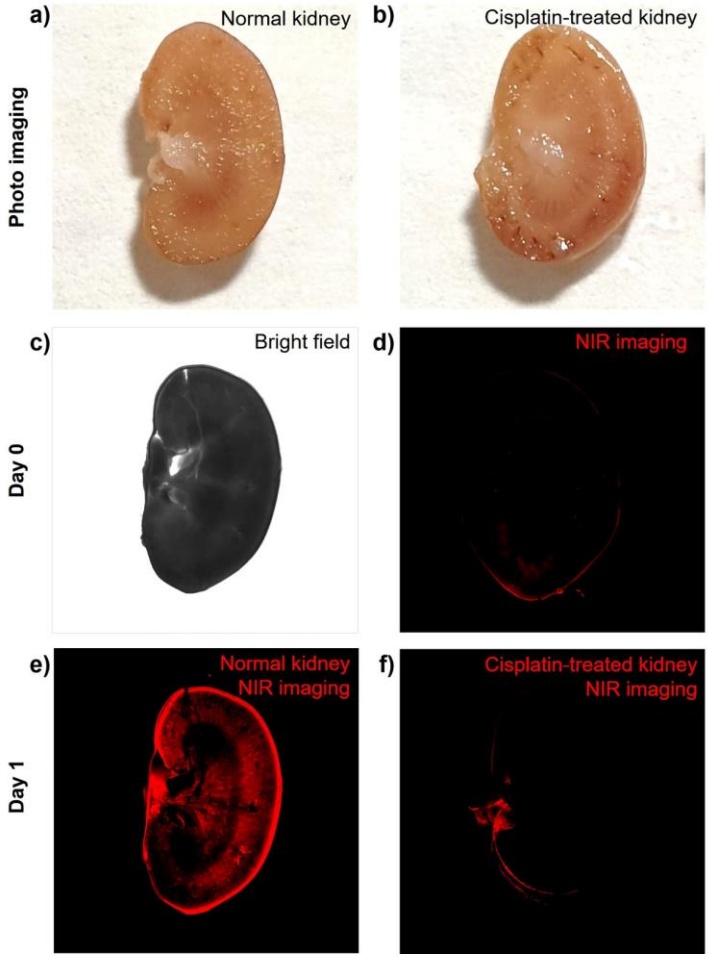

Figure S10. In situ growth and NIR fluorescence imaging of GS-AuNPs in normal and disease (cisplatin-treated) kidney. The disease kidney model with acute injury was conducted by the intravenous injection of cisplatin into female balb/c mice (6 – 8 weeks old) with the overall dose schedule of cisplatin 14 mg/kg body weight (2 mg/kg every day, ×7, n = 3), which was estimated at about the maximal tolerated dose (MTD) of cisplatin multiple treatment.[4, 5] The repeated cisplatin exposure is known to induce severe acute kidney injury (necrosis and apoptosis of tubule cells)[6] by depleting intracellular GSH, increasing oxidative stress and impairing the structure and enzymatic activity of mitochondria.[7] In contrast, the normal kidney was acquired as control group after the successive treatment of equivalent saline buffer (every day, ×7, n = 3). **a-b)** Photo imaging of the tissue slides (1 mm in thickness) of normal kidney and disease (cisplatin-treated) kidney. The kidneys were removed from the mice and then fixed in 10% formalin solution for over 24 h. **c**-**f**) NIR imaging of the kidney tissues before (Day 0, **c**, bright field, **d**, NIR imaging background) and after (Day 1, **e**, NIR imaging of normal kidney, **f**, NIR imaging of the cisplatin-treated

kidney) the in situ growth of GS-AuNPs. Exposure time: 2s. Consistent with **Fig. 3**, there was strong NIR signal on the normal kidney tissue after the AuNP growth on Day 1 (**e**). Meanwhile, there was no observable enhancement of NIR signal from the disease kidney tissue, which may attribute to the cisplatin-induced impairment of mitochondrial structures in the renal tubule cells. The results suggested that the in situ growth and labeling of AuNPs may be used for ex vivo disease detection and diagnosis once with the rational design of the nanoparticle staining.

References

1. Gomes, J. F.; Garcia, A. C.; Ferreira, E. B.; Pires, C.; Oliveira, V. L.; Tremiliosi-Filho, G.; Gasparotto, L. H. *Phys. Chem. Chem. Phys.* **2015,** 17, (33), 21683-21693.

2. Wei, H.; Wang, Z.; Zhang, J.; House, S.; Gao, Y.-G.; Yang, L.; Robinson, H.; Tan, L. H.; Xing, H.; Hou, C. *Nat. Nanotechnol.* **2011,** 6, (2), 93.

3. Yang, S.; Sun, S.; Zhou, C.; Hao, G.; Liu, J.; Ramezani, S.; Yu, M.; Sun, X.; Zheng, J. *Bioconjugate Chem.* **2015,** 26, (3), 511-519.

4. Newman, M. S.; Colbern, G. T.; Working, P. K.; Engbers, C.; Amantea, M. A. *Cancer Chemother. Pharmacol.* **1999,** 43, (1), 1-7.

5. Kurihara, N.; Kubota, T.; Hoshiya, Y.; Otani, Y.; Watanabe, M.; Kumai, K.; Kitajima, M. *J. Surg. Oncol.* **1996,** 61, (2), 138-142.

6. Arany, I.; Safirstein, R. L. *Semin. Nephrol.* **2003,** 23, (5), 460-464.

7. Zsengellér, Z. K.; Ellezian, L.; Brown, D.; Horváth, B.; Mukhopadhyay, P.; Kalyanaraman, B.; Parikh, S. M.; Karumanchi, S. A.; Stillman, I. E.; Pacher, P. *J. Histochem. Cytochem.* **2012,** 60, (7), 521-529.